

Free space TEM transmission lines radiation losses model

Reuven Ianconescu*, Vladimir Vulfin†

*Shenkar College of Engineering and Design, Ramat Gan, Israel, riancon@gmail.com

†Ben-Gurion University of the Negev, Beer Sheva 84105, Israel, vlad2042@yahoo.com

Abstract—There are three kind of losses in transmission lines: ohmic, dielectric and radiation losses. While the first two are local phenomena which are easy to model, there is no model for the radiation losses yet. This work derives a radiation model for two conductors transmission lines in free space, within the RLGC transmission lines model. The analytic results are confirmed by successful comparison with ANSYS commercial software simulation results, and comparisons with other published results.

Index Terms—electromagnetic theory, guided waves, TEM waveguides, radiation losses model, EM Field Theory.

I. INTRODUCTION

While ohmic and dielectric losses in transmission lines (TL) have a simple representation within the RLGC “telegraph” model, due to their local characteristics [1]–[4], there is no radiation losses model for TL, although some attempts to study this subject have been done [5]–[8].

The aim of this work is to analyze the radiation process in two conductors TL in free space with the scope of incorporating the radiation losses phenomenon into the RLGC model of the TL. Some preliminary results have been presented in [9], [10].

The methodology we use is the same one used to calculate any small losses: we use the lossless (0’th order solution) for the electric current to derive the losses. This methodology is used to derive the ohmic and dielectric losses [1]–[4], and the same approach is used in different radiation schemes from free electrons: one uses the 0’th order current (which is unaffected by the radiation) to calculate the radiation [11]–[13].

This approach allows us to use the one dimensional (undisturbed) solution for the TL, and is justified as long as the guided waves travel only along the TL (\hat{z} direction), i.e. the transverse dimension is much smaller than the wavelength, so that we deal only with the TEM mode. To be mentioned that this is the typical usage of two conductors TL.

To derive a radiation model, one needs to find a radiation resistance per length unit R_{rad} to be added to the RLGC model of the TL. This radiation resistance per length unit is meant to reflect the amount of radiated power from different sections of the TL. The problem is that the radiation is a global effect of constructive interference of different contributions along the line, so that physically, one cannot state from which location on the TL the power is radiated. Hence to achieve this goal one has to formulate an equivalent “localization” by checking how an *additional* line length changes the radiated power, and

as we shall see this additional radiation is not proportional to the increase in the line length, and may even be negative.

Because this subject has never been fully analyzed, some “myths” developed, like “matched TL do not radiate”, or “only open ended TL radiate”. The first is certainly based on the fact that a “matched load absorbs all the power” - but to be more accurate: “it absorbs all the power that reaches it”, a matched load does not prevent radiation [6]. Anyhow, this work shows that those myths are incorrect. We do not consider a specific termination in this work, but rather consider the general case of any type of termination, and as we shall see, the difference between open and matched TL, in what concerns radiation, is only a small factor.

It should be also mentioned that power loss from TL is also affected by nearby objects interfering with the fields, line bends, irregularities, etc. This is certainly true, but those affect *not only* the radiation, *but also* the basic, “ideal” TL model in what concerns the characteristic impedance, the propagation wave number, etc. Those non-ideal phenomena are *not considered* in the current work, which derives a radiation-losses model for ideal, non bending, fixed cross section TL.

We consider a general configuration of two ideal conductors TL in free space, of any uniform transverse cross section size much smaller than the wavelength, shown in Figure 1. We

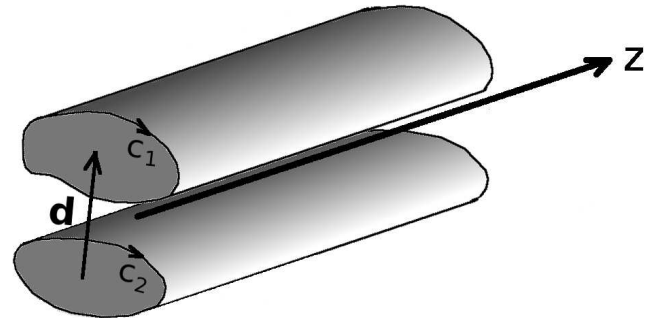


Fig. 1. A basic configuration of a two ideal conductors TL, with a well defined separation between the conductors. The surface current distributions on the contours of the conductors is known from electrostatic considerations, and the total current is the same on both conductors but with opposite signs. The arrow shows the vector distance between the center of the surface current distributions, named \mathbf{d} , obtained for a twin lead equivalent (see Appendix A). $c_{1,2}$ are the contours of the “upper” and “lower” conductors, respectively. We consider the case of $kd \ll 1$, k being the wavenumber.

show in Appendix A that for the *purpose of calculating the radiated power* and hence the far fields, any two conductors

TL with cross section much smaller than the wavelength may be represented by a twin lead configuration, with a separation distance d , as shown in Figure 2. Typically, one wants to

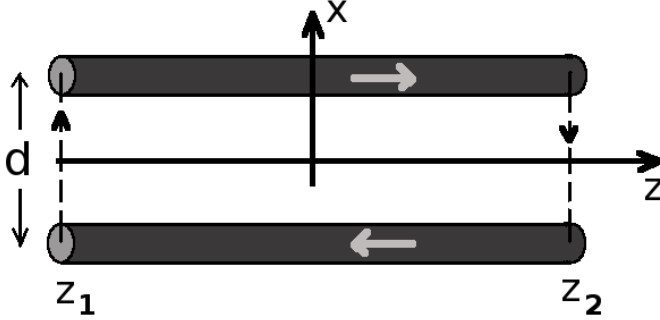


Fig. 2. The transmission line is modeled as a twin lead in free space, with distance d between the conductors. The currents in the transmission line flow in the z direction at $x = \pm d/2$ and they contribute to the magnetic vector potential A_z . The termination currents (source or load) flow in the x direction and contribute the magnetic vector potential A_x . The arrows on the conductors show the conventional directions of those currents. The wires appear in the figure with finite thickness, but are considered of 0 radius. The transmission line goes in the z direction from z_1 to z_2 .

calculate the radiated power relative to the power carried by a forward wave P_{rad}/P^+ , hence we shall need the characteristic impedance which has to be calculated for the *actual* cross section (not the twin lead).

The work is organized as follows: In Section II we calculate the power radiated by a finite matched line of length $2L$, and generalize the result for a non matched TL. In Section III we validate the analytic results of Section II by comparing them with ANSYS commercial software simulation results, and with published results obtained by other authors.

The analytic results from Section II suffice in principle to formulate a radiation-losses model, but to get a better insight into the origin of the radiation, and an additional validation and interpretation of the results, we analyze in Section IV an infinite and semi-infinite TL, and show the connection between the power radiated by a finite TL and this radiated by a semi-infinite TL.

In Section V we derive the RLGC model for the radiation losses, which consists in a series radiation resistance per length unit R_{rad} which starts at a termination and varies along the TL. The calculation of the radiation model requires the knowledge of the separation distance d in the twin lead representation for the given cross section, and in Appendix B we show how to perform this computation.

The work is ended with some concluding remarks.

Note: through this work, the phasor amplitudes are RMS values, hence there is no 1/2 in the expressions for power. Also, it is worthwhile to mention that the results of this work depend on physical sizes relative to the wavelength, and hence are valid for all frequencies.

II. POWER RADIATED FROM A FINITE TL

A. Matched TL

We calculate in this subsection the power radiated from a TL of length $2L$, carrying a forward wave, represented by the

current $I(z) = I^+ e^{-jkz}$. We set $z_1 = -L$ and $z_2 = L$ in the expression for the z directed magnetic vector potential in Eq. (A.13) from Appendix A, and obtain in spherical coordinates:

$$A_z = \mu_0 G(r) F_{(z)}(\theta, \varphi) \quad (1)$$

where G is the 3D Green's function defined in (Eq. (A.2)), and

$$F_{(z)}(\theta, \varphi) = jI^+ 2Lkd \sin \theta \cos \varphi \text{sinc}[kL(1 - \cos \theta)] \quad (2)$$

is the directivity function, and the subscript (z) denotes the contribution from the z directed currents. The sinc function is defined $\text{sinc}(x) \equiv \sin x/x$. To obtain the far fields (those decaying like $1/r$), the ∇ operator is approximated by $-jk\hat{\mathbf{r}}$ and one obtains:

$$\mathbf{H}_{(z)} = \frac{1}{\mu_0} \nabla \times (A_z \hat{\mathbf{z}}) = jkG(r) F_z(\theta, \varphi) \sin \theta \hat{\boldsymbol{\varphi}} \quad (3)$$

and $\mathbf{E}_{(z)} = \eta_0 \mathbf{H}_{(z)} \times \hat{\mathbf{r}}$, where $\eta_0 = \sqrt{\mu_0/\epsilon_0} = 120\pi\Omega$ is the free space impedance. For the contribution of the x directed end currents we sum the results for the x directed magnetic vector potential from Eq. (A.16) in Appendix A (setting $z_1 = -L$ and $z_2 = L$), obtaining

$$A_x = \mu_0 G(r) F_{(x)}(\theta, \varphi) \quad (4)$$

where

$$F_{(x)}(\theta, \varphi) = 2jI^+ d \sin[kL(1 - \cos \theta)] \quad (5)$$

is the directivity function, and the subscript (x) denotes the contribution from the x directed currents. The fields from the x directed end currents are calculated, obtaining

$$\mathbf{H}_{(x)} = \frac{1}{\mu_0} \nabla \times (A_x \hat{\mathbf{x}}) = -jkG(r) F_{(x)}(\cos \theta \cos \varphi \hat{\boldsymbol{\varphi}} + \sin \varphi \hat{\boldsymbol{\theta}}) \quad (6)$$

and $\mathbf{E}_{(x)} = \eta_0 \mathbf{H}_{(x)} \times \hat{\mathbf{r}}$. Now summing the fields contributed by the z directed currents with those contributed by the x directed currents, we obtain $\mathbf{H} = \mathbf{H}_{(z)} + \mathbf{H}_{(x)}$:

$$\mathbf{H} = jkG(r) [\hat{\boldsymbol{\varphi}}(F_z \sin \theta - F_x \cos \theta \cos \varphi) - \hat{\boldsymbol{\theta}} F_x \sin \varphi] \quad (7)$$

and

$$\mathbf{E} = \mathbf{E}_{(z)} + \mathbf{E}_{(x)} = \eta_0 \mathbf{H} \times \hat{\mathbf{r}} \quad (8)$$

The far Poynting vector $\mathbf{S} = \mathbf{E} \times \mathbf{H}^*$ comes out

$$\begin{aligned} \mathbf{S} = & \frac{\eta_0 k^2 \hat{\mathbf{r}}}{16\pi^2 r^2} (|F_z \sin \theta - F_x \cos \theta \cos \varphi|^2 + \\ & |F_x \cos \theta \cos \varphi|^2) = \frac{\hat{\mathbf{r}} \eta_0 k^2 d^2 |I^+|^2}{4\pi^2 r^2} \sin^2 [2kL \sin^2(\theta/2)] \end{aligned} \quad (9)$$

so that the total radiated power is

$$P_{\text{rad}} = \int_0^{2\pi} \int_0^\pi \sin \theta d\theta d\varphi r^2 \hat{\mathbf{r}} \cdot \mathbf{S}, \quad (10)$$

which comes out

$$P_{\text{rad}} = 60\Omega |I^+|^2 (kd)^2 [1 - \text{sinc}(4kL)]. \quad (11)$$

The radiation pattern function is calculated from the radial pointing vector (Eq. 9) and the total power in Eq. 11, using by $D = 4\pi r^2 S_r / P_{rad}$ and comes out

$$D(\theta) = 2 \frac{\sin^2[kL(1 - \cos\theta)]}{[1 - \text{sinc}(4kL)]}, \quad (12)$$

and the radiated power relative to the forward wave propagating power ($P^+ = |I^+|^2 Z_0$) is given by

$$\frac{P_{rad}}{P^+} = \frac{60\Omega}{Z_0} (kd)^2 [1 - \text{sinc}(4kL)], \quad (13)$$

This is the central result of this paper, on which the radiation losses model is based. The calculation of the relative radiated power requires the knowledge of two parameters: the separation distance in the twin lead representation d (relative to the wavelength), and the characteristic impedance of the actual cross section Z_0 , and in Appendix B we show examples of how to calculate this two parameters for different cross sections.

In the following subsection we generalize the radiation losses for a TL with any termination.

B. Generalization for non matched line

We generalize here the result (11) obtained for the losses of a finite TL carrying a forward wave to any combination of waves, as follows:

$$I(z) = I^+ e^{-jkz} + I^- e^{jkz} \quad (14)$$

where I^+ is the forward wave phasor current, as used in the previous subsection and I^- is the backward wave phasor current, still defined to the right in the ‘‘upper’’ line in Figure 2.

The solution for a backward moving wave (only) on the finite TL, with a current phasor amplitude I^- can be found by first solving for a *reversed* z axis in Figure 2, i.e. a z axis going to the left, replacing in the solution $I^+ \rightarrow -I^-$. But this defines exactly the same configuration for the backward wave, as the original z axis defined for a forward wave, hence resulting in the same solution in Eqs. (7) and (8). Now to express the solution for the backward wave in the original coordinates, defined by the right directed z axis, one has to replace: $\theta \rightarrow \pi - \theta$, $\varphi \rightarrow -\varphi$, and therefore also $\hat{\theta} \rightarrow -\hat{\theta}$ and $\hat{\varphi} \rightarrow -\hat{\varphi}$, and finally sum the fields of the forward and backward waves. One obtains for the contribution of the z directed currents:

$$\mathbf{H}_{(z)} = -\hat{\varphi} k G(r) 2kLd \sin^2 \theta \cos \varphi (I^+ \text{sinc}[kL(1 - \cos\theta)] + I^- \text{sinc}[kL(1 + \cos\theta)]) \quad (15)$$

and the x directed currents:

$$\mathbf{H}_{(x)} = kG(r) 2d (\hat{\varphi} \cos \theta \cos \varphi + \hat{\theta} \sin \varphi) (I^+ \text{sinc}[kL(1 - \cos\theta)] - I^- \text{sinc}[kL(1 + \cos\theta)]) \quad (16)$$

Note that this solution is general and covers also the case of resonant TL with open ends, which will be compared with published results in the Section III-B. In such case, $I^+ = I^-$,

and for the lowest resonance, $kL = \pi/2$, so that the current distribution defined in (14) becomes

$$2I^+ \cos(kz) \quad (17)$$

and is 0 at the terminations $z = \pm L$. In such case also $\mathbf{H}_{(x)}$ in (16) is 0 because $\sin[(\pi/2)(1 - \cos\theta)] = \sin[(\pi/2)(1 + \cos\theta)]$ for any θ .

Going on with the general case, the far Poynting vector is

$$\mathbf{S} = \hat{\mathbf{r}} \eta_0 \frac{4(kd)^2}{16\pi^2 r^2} \{ |I^+|^2 \sin^2 [2kL \sin^2(\theta/2)] + |I^-|^2 \sin^2 [2kL \cos^2(\theta/2)] + 2 \cos(2\varphi) \sin [2kL \sin^2(\theta/2)] \sin [2kL \cos^2(\theta/2)] \Re\{I^+ I^{-*}\} \} \quad (18)$$

The interference between the waves does not contribute to the radiated power (because $\int_0^{2\pi} d\varphi \cos(2\varphi) = 0$). The radiated power comes out

$$P_{rad} = 60\Omega (kd)^2 (|I^+|^2 + |I^-|^2) [1 - \text{sinc}(4kL)], \quad (19)$$

so that the powers radiated by the forward and backward waves add up, hence a radiation losses model defining a radiation resistance per length unit for the forward wave, covers the case of an existing backward wave.

In the next section we validate the analytic results obtained in this section, using ANSYS commercial software simulation and additional published results on radiation losses from TL.

III. VALIDATION OF THE ANALYTIC RESULTS

A. Comparison with ANSYS simulation results

We compare in this subsection the relative radiated power from a two conductor TL (Eq. 13) carrying a forward wave, with the relative radiation losses results obtained from ANSYS commercial software simulation. For the comparison we use the cross section of two parallel cylinders, for which the analytic solution is known from image theory [1]–[4]. The cross section is shown in Figure 3. The diameters of the cylinders are $2a = 0.0203\lambda$, and the distance between their centers is $s = 0.02872\lambda$, where the wavelength $\lambda = 6.25\text{cm}$, corresponding to the frequency of 4.8GHz. The distance between the image currents (shown as red points in Figure 3) is the separation distance d in the twin lead model, given by

$$d = \sqrt{s^2 - (2a)^2} = 0.0203\lambda, \quad (20)$$

and the characteristic impedance is

$$Z_0 = \frac{\eta_0}{\pi} \ln \left(\frac{d+s}{2a} \right) = 105.6\Omega \quad (21)$$

We simulated the configuration in Figure 3 using ANSYS-HFSS commercial software, in the frequency domain, FEM technique. The box surface enclosing the device constitutes a radiation boundary, implying absorbing boundary conditions (ABC), used to simulate an open configuration that allows waves to radiate infinitely far into space. ANSYS HFSS ABC, absorbs the wave at the radiation boundary, essentially ballooning the boundary infinitely far away from the structure. The enclosing box surface has to be located at least a quarter wavelength from the radiating source. For the frequency of

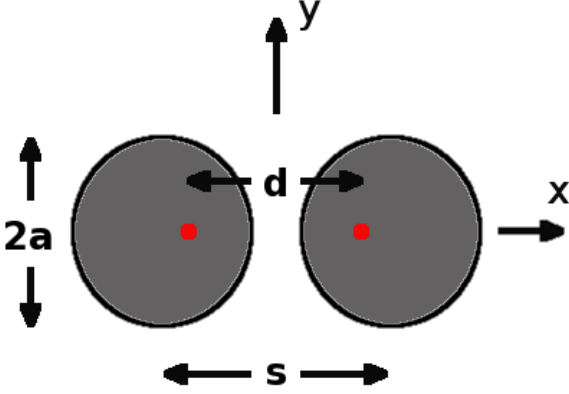


Fig. 3. Cross section of two parallel cylinders: the distance between the centers is $s = 0.02872$, and the diameters are $2a = 0.0203$ wavelengths. The red points show the current images which define the twin lead representation, and the distance between them $d = 0.0203$ wavelengths is calculated in Eq. (20).

4.8GHz we used, the wavelength is 6.25cm, and we chose the box sides 7.5cm in the x and y directions, and the TL length plus 2.5cm on each side in the z direction. For the interface to the device we used lumped ports, which define perfect H boundaries everywhere on the port plane, so that the E field on the port plane (outside the conductors) is perpendicular to the conductors.

We obtained from the simulation S matrices defined for a characteristic impedance of 50Ω at both ports, for different lengths of the transmission line. By symmetry, the S matrix has the form

$$S = \begin{pmatrix} \Gamma & \tau \\ \tau & \Gamma \end{pmatrix}, \quad (22)$$

from which one may calculate the ABCD matrix of the TL [1], [20], [21]. We need only the A element from the matrix:

$$A = \frac{1}{2} [\tau + (1 - \Gamma^2)/\tau] \quad (23)$$

from which we compute the delay angle of the TL

$$\Theta = \arccos(A) \quad (24)$$

The radiated power, relative to the load power is obtained by

$$\frac{P_{rad}}{P^+} = -2\text{Im}\{\Theta\}, \quad (25)$$

where Im is the imaginary part and $\text{Im}\{\Theta\} < 0$ always.

In Table I and Figure 4 we compare the analytic result in Eq. (13) with the result obtained from simulation Eq. (25), for a fixed frequency of 4.8GHz and different TL lengths. We see that the simulation confirms well the theoretical result, with an average absolute relative error of 4.77%. The biggest relative errors are at the short TL, where the relative radiation losses are low, and hence more difficult to reproduce accurately with the simulation. For example, if we exclude the shortest TL length of 0.08λ from the comparison, the average absolute relative error is 2.62%, or if we exclude the 2 shortest points of 0.08 and 0.16λ from the comparison, it drops to 1.66%.

TABLE I
RELATIVE RADIATION LOSSES FOR A MATCHED TL P_{rad}/P^+ :
COMPARISON BETWEEN THE ANALYTIC RESULT IN EQ. (13) AND THE
SIMULATION RESULT IN EQ. (25) FOR DIFFERENT TL LENGTHS, GIVEN IN
UNITS OF WAVELENGTHS.

TL length	ANSYS simulation (Eq. 25)	theoretical (Eq. 13)
0.08	0.0019632	0.0014787
0.16	0.005796	0.0050787
0.24	0.009502	0.0088506
0.4	0.011115	0.010982
0.6	0.007987	0.0080696
0.8	0.0098782	0.0097743
0.96	0.0095756	0.0096031
1.12	0.0081986	0.0085796
1.2	0.0086461	0.0088744
1.28	0.0093663	0.0094457
1.44	0.0095891	0.0095837
1.6	0.0086654	0.0087976
1.76	0.0092164	0.0092867
1.92	0.0097469	0.0095575
2.08	0.0090464	0.0089361

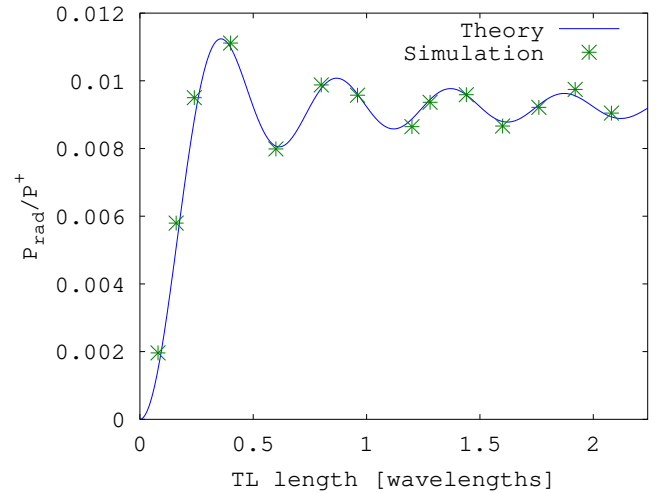


Fig. 4. Relative radiation losses for a matched TL P_{rad}/P^+ : comparison between the analytic result in Eq. (13) and the simulation result in Eq. (25) for different TL lengths in units of wavelengths.

B. Comparison with Ref. [5]

In 1923 Manneback [5] published a paper “Radiation from transmission lines” which calculated the power radiated by two thin wires of length l (equivalent to our $2L$), and separation d , in resonance, having open terminations. The author considered the current

$$I_m \cos(k_n z) \sin(\omega_n t) \quad (26)$$

where $k_n = \pi n/l$ and $\omega_n = ck_n$ for odd n (as defined in Eq. 3 of [5]). Note that the time dependence has been explicitly written in [5] and the calculations have been done in time domain, but using a fixed frequency, hence they are completely equivalent to our phasor calculations. The result for the radiated power is given in Eq. 11 of [5], rewritten here for convenience

$$P_{rad} = 15\Omega(kd)^2 I_m^2 \quad (27)$$

We compare this with our result (19). $kl = n\pi$ is in our notation $kL = n\pi/2$ hence the sinc function in Eq. (19)

results 0. As mentioned in Section II-B this resonant case implies $I^+ = I^-$, so that the current is given in Eq. (17), hence Eq. (19) results in $120\Omega(kd)^2|I^+|^2$.

The value I_m in Eq. (26) is the amplitude of the current, i.e. the RMS value times $\sqrt{2}$. We use RMS values (as mentioned in the introduction) hence the equivalence between Eq. (26) and Eq. (17) is by setting $I_m = 2\sqrt{2}|I^+|$, and using this equivalence, Eq. (19) reduces *exactly* to Eq. (27).

To be mentioned that our results are general, covering all cases of terminations, or any combination of waves, and we showed in this subsection how our general result reduces correctly to the result for a private case of resonance.

C. Comparison with Ref. [6]

Another comparison is with Bingeman's work from 2001 [6], in which the method of moments (MoM) has been used to calculate the radiation from two thin wires of diameter $2a = 5\text{mm}$, length $2L = 10\text{m}$ and separated at a distance of $d = 1\text{m}$. The characteristic impedance is given by Eq. (21) (but given $d \gg a$ one may use $s = d$, see Eq. (20)) and results in $Z_0 = 720\Omega$, as calculated at the beginning of Ref. [6]. In absence of other losses, the author derived the radiated power as the difference between the power carried by the TL and the power reaching the load.

The first calculation is the power radiated by a matched TL, fed by a power of 1000W, for frequencies $f = 2, 5, 7, 10, 15$ and 20MHz. For the power of 1000W, the RMS value of the forward current to set in Eq. (11) is $|I^+| = \sqrt{1000/Z_0} = 1.1785\text{A}$, and we use $k = 2\pi f/c$ for the above frequencies. The numerical results for this case are given in Table 1 of Ref. [6], and we compare those results to ours, in Table II and Figure 5. We see a good match for

TABLE II
COMPARISON BETWEEN THE RADIATED POWER [W] FOR A MATCHED LINE FROM TABLE 1 OF REF. [6] WITH OUR RESULTS FOR A MATCHED LINE IN EQ. (11) FOR DIFFERENT FREQUENCIES.

Frequency [MHz]	Ref. [6]	theoretic (Eq. 11)
2	0	0.0165
5	1	0.5359
7	2	1.6641
10	4	4.4111
15	8	8.2246
20	13	13.1101

the high frequencies (big electric delay), and it deteriorates at small electric delays. But the result 0 for the frequency of 2MHz is clearly incorrect, so we may understand that the accuracy of the results in Ref [6] is low at small electric delays, for which the relative radiated power is small.

Another calculation in Ref. [6] is for a non matched TL, with end loads $R_L=10, 50, 500\Omega, 1, 5, 10,$ and $50k\Omega$, all cases at frequency 10MHz, carrying a net power of 1000W. We shall compare those results with the results of Eq. (19). First $k = 2\pi f/c = 0.2094[1/\text{m}]$ is fixed, and we calculate for each load resistance R_L

$$|\Gamma| = \left| \frac{R_L - Z_0}{R_L + Z_0} \right|, \quad (28)$$

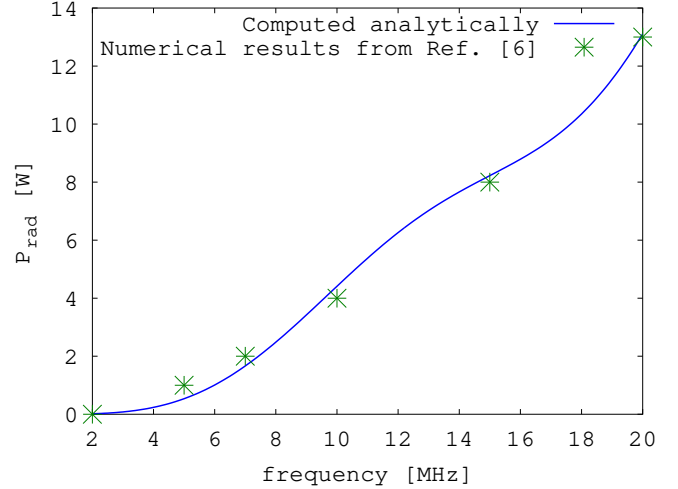


Fig. 5. Comparison between the radiated power for a matched line from Table 1 of Ref. [6] with our results for a matched line in Eq. (11) for different frequencies.

from which the forward power values for each case are given by

$$P^+ = \frac{P}{1 - |\Gamma|^2} = \frac{1000}{1 - |\Gamma|^2}. \quad (29)$$

The forward current values for each case are given by $|I^+| = \sqrt{P^+/Z_0}$ and the backward current values for each case are given by $|I^-| = |\Gamma||I^+|$. Setting the values in Eq. (19), we compare the results of Ref. [6] for the unmatched line at 10MHz (Table 2 in [6]), with the results of Eq. (19) in Table III and Figure 6. The match between the results is

TABLE III
COMPARISON BETWEEN THE RADIATED POWER [W] FOR A NON MATCHED LINE FROM TABLE 2 OF REF. [6] WITH OUR THEORETICAL RESULTS FOR A NON MATCHED LINE IN EQ. (19) FOR DIFFERENT LOAD RESISTANCES.

Load R_L [Ω]	Ref. [6]	theoretical (Eq. 19)
10	140	158.83
50	32	31.91
500	5	4.70
1k	5	4.65
5k	15	15.63
10k	29	30.79
50k	128	153.19

good, except for the first and last cases, in which the radiated power is big and approaches the order of magnitude of the net power (1000W). This may be due to the limitations of the current theory to small losses that almost do not affect the basic electromagnetic solution (see Introduction).

D. Comparison with Ref. [7]

In 2006 Nakamura et. al. published the paper "Radiation Characteristics of a Transmission Line with a Side Plate" [7] which intends to reduce radiation losses from TLs using a side plate. The side plate is a perfect conductor put aside the transmission line, to create opposite image currents, and hence reduce the radiation.

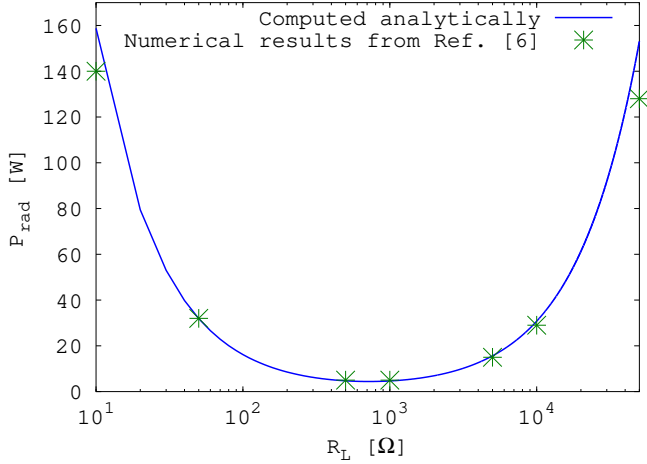


Fig. 6. Comparison between the radiated power for a non matched line from Table 2 of Ref. [6] with our results for a non matched line in Eq. (19) for different load resistances.

The authors first derived the radiation from a TL without the side plate, obtaining an integral (Eq. 20 in Ref. [7]) which they computed numerically. The numerical integration result is shown in Figure 6 of Ref. [7], where the solid line represents the free space case.

We compare our analytic result in Eq. (11), with the numerical result shown in Figure 6 of Ref. [7]. First, I_0 in [7] is a forward current, and from Eq. (19) in [7], it is evident that they used RMS values. They used $I_0 = 1\text{A}$, hence we set $|I^+| = 1\text{A}$ in Eq. (11). $2h$ is the distance between the conductors in [7], equivalent to d in this work, and they used $h\lambda = 0.1$, therefore $(kd)^2 = (4\pi h/\lambda)^2 = 1.5791$ in Eq. (11), so that the total radiated power for the case displayed in Figure 6 of Ref. [7] is

$$P_{rad} = 60 \times 1 \times 1.5791 [1 - \text{sinc}(4kL)] = 94.746 [W] \left[1 - \text{sinc} \left(\frac{2L}{\lambda} 4\pi \right) \right], \quad (30)$$

and we wrote the argument of the sinc function in terms of $2L/\lambda$, i.e. the TL length in wavelengths. This result is displayed in Figure 7, in which we show the radiated power as function of the TL length in wavelengths. The authors did not supply the numerical data to reproduce Figure 6 of Ref. [7], and we did not want to copy the figure into this work for comparison, but we checked very carefully that indeed our calculation shown in Figure 7 *completely overlaps* the solid line in Figure 6 of Ref. [7].

We compare as well the radiation patterns obtained in [7] with ours (Eq. 12) in Figure 8. We remark that $D(\theta)$ is not symmetric around $\theta = \pi/2$ in general, but for the cases $kL = n\pi/2$ (integer n), i.e. the TL length is a multiple integer of half wavelength, displayed in Figure 8, $D(\theta)$ is symmetric around $\theta = \pi/2$, because $\sin^2(n\pi/2+x) = \sin^2(n\pi/2-x)$ for any x . The radiation patterns in Figure 8 are *identical* to the parallel cases shown in Figure 5, panel(a) of Ref. [7], up to a rotation of 90° around the y axis (because the definitions of the z and x axes in [7] are swapped relative to our definitions).

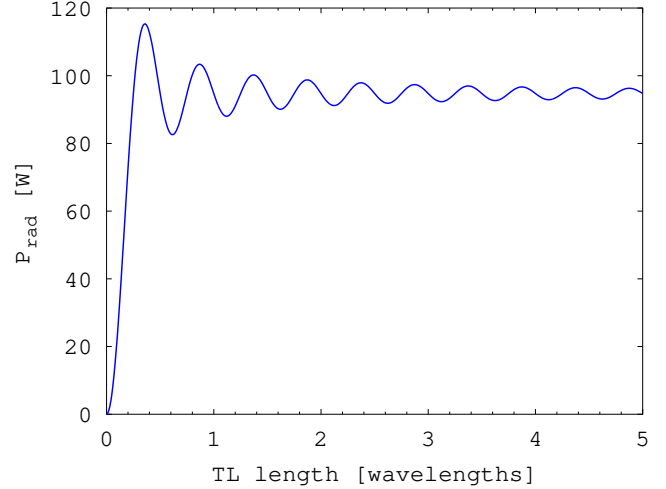


Fig. 7. Recalculation of the solid line in Figure 6 of Ref. [7], using Eq. (11).

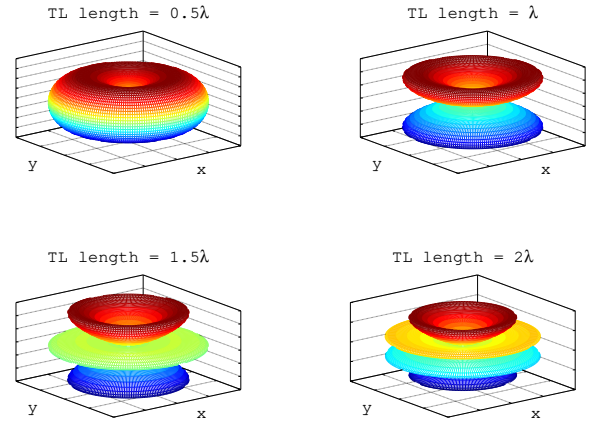


Fig. 8. Radiation pattern calculated from Eq. (12) for the cases of TL lengths $n\lambda/2$, for $n=1$ to 4. They are identical to the parallel cases shown in Figure 5, panel(a) of Ref. [7] (up to a rotation of 90° around the y axis, due to swapped definitions of the x and z axes in [7]).

It is worthwhile to remark that the radiation pattern (Eq. 12) does not depend on the distance between the conductors d (or $2h$ in [7]), hence the annotation of $h/\lambda = 0.1$ in Figure 5 of Ref. [7] is redundant, and probably has been added to the caption because the authors computed the radiation patterns numerically for $h/\lambda = 0.1$, without deriving an analytic expression.

IV. INFINITE AND SEMI-INFINITE TL ANALYSIS

As we know, there are no infinite or semi-infinite TL in reality, but the literature considers those kind of TL as limiting cases, and as we shall see, the analysis of the infinite and semi-infinite TL supplies an additional insight and validation of the results obtained in the Section II.

For an infinite TL, carrying a forward wave, we set $z_1 = -L$ and $z_2 = L$ in the result (A.13) and considering $L \rightarrow \infty$ (i.e.

for finite z and ρ , $L \gg |z|, \rho$ we obtain

$$A_z = \frac{\mu_0 I^+}{4\pi} d \cos \varphi \frac{2e^{-jkz}}{\rho}, \quad (31)$$

from which

$$\mathbf{H} = \frac{1}{\mu_0} \nabla \times \mathbf{A} = \frac{e^{-jkz}}{2\pi} \frac{I^+ d}{\rho^2} [-\hat{\rho} \sin \varphi + \hat{\varphi} \cos \varphi] \quad (32)$$

and

$$\mathbf{E} = \frac{1}{j\omega\epsilon_0} \nabla \times \mathbf{H} = \eta_0 \frac{e^{-jkz}}{2\pi} \frac{I^+ d}{\rho^2} [\hat{\rho} \cos \varphi + \hat{\varphi} \sin \varphi], \quad (33)$$

Certainly, we do not need here the contributions of the x directed currents (A.16). The Poynting vector is

$$\mathbf{S} = \mathbf{E} \times \mathbf{H}^* = \eta_0 \frac{1}{4\pi^2} \frac{|I^+|^2 d^2}{\rho^4} \hat{\mathbf{z}} \quad (34)$$

Clearly, an infinite line (even having the geometry of an open structure), never radiates in the usual sense, i.e. as an escaping power. Calculating here the ‘‘radiated’’ power just results in the power carried by the TL - this is true if the space around the TL is completely free of any objects that come in contact with the fields of the TL, and this is the assumption in this work, as mentioned in the introduction.

Therefore, any radiation from a TL must emerge from a termination, and we further analyze a semi-infinite TL from $-\infty$ to 0 , carrying a forward moving wave. We note that in this case we have to consider the contribution of the x directed current at the termination at $z = 0$ in addition to the z directed currents contributions. Starting with the z directed currents contributions, we set $z_1 = -L$ and $z_2 = 0$ in Eq. (A.13) and considering $L \rightarrow \infty$ we obtain

$$A_z = \frac{\mu_0 I^+}{4\pi} d \cos \varphi \left[\frac{2e^{-jkz}}{\rho} - \frac{\rho}{r-z} \frac{e^{jkr}}{r} \right] \equiv A_{z \text{ plane}} + A_{z \text{ spherical}}. \quad (35)$$

The left expression describes the plane wave we got for the infinite line (Eq. 31), and the right expression describes a spherical wave emerging from the end of the transmission line at the coordinates origin.

At $z > 0$, the plane wave and its singularity at $\rho = 0$ has to disappear, and one can easily check that the spherical wave cancels it. For $\rho \ll z$, approximating the spherical wave to first order, we have $r \approx z + \frac{\rho^2}{2z}$, so that $r - z \approx \frac{\rho^2}{2z}$ and the spherical wave reduces to $-\frac{2e^{-jkz}}{\rho}$.

Hence, the plane wave ‘‘exists’’ only at $z < 0$, and is absorbed by the matched load at $z = 0$, as expected, and the radiated power may be calculated from the spherical wave emerging from the origin, rewritten fully in spherical coordinates:

$$A_{z \text{ spherical}} = \mu_0 F_{(z)}(\theta, \varphi) G(r), \quad (36)$$

where

$$F_{(z)}(\theta, \varphi) = -I^+ d \cos \varphi \frac{\sin \theta}{1 - \cos \theta}, \quad (37)$$

is the directivity function. We calculate now the radiating electric and magnetic fields, i.e. the part of the fields which

decays like $1/r$. This is done like in Eqs. (32) and (33) after approximating $\nabla \simeq -jk\hat{\mathbf{r}}$, obtaining

$$\mathbf{H}_{(z)} = jk F_{(z)}(\theta, \varphi) \sin \theta G(r) \hat{\varphi}, \quad (38)$$

and $\mathbf{E}_{(z)} = \eta_0 \mathbf{H}_{(z)} \times \hat{\mathbf{r}}$.

Now we calculate the contribution of the end current at $z_2 = 0$, using Eq. (A.16) in Appendix A, we obtain

$$A_x = \mu_0 F_{(x)}(\theta, \varphi) G(r), \quad (39)$$

where the directivity function $F_{(x)}$ is

$$F_{(x)}(\theta, \varphi) = -I^+ d, \quad (40)$$

The fields are $\mathbf{H}_{(x)} = (-jk\hat{\mathbf{r}}) \times (A_x \hat{\mathbf{x}}) / \mu_0$

$$\mathbf{H}_{(x)} = -jk(\cos \theta \cos \varphi \hat{\varphi} + \sin \varphi \hat{\theta}) G(r) F_{(x)}, \quad (41)$$

and $\mathbf{E}_{(x)} = \eta_0 \mathbf{H}_{(x)} \times \hat{\mathbf{r}}$. Adding up the fields we obtain $\mathbf{H} = \mathbf{H}_{(z)} + \mathbf{H}_{(x)}$

$$\mathbf{H} = jkG(r)[\hat{\varphi}(F_{(z)} \sin \theta - F_{(x)} \cos \theta \cos \varphi) - \hat{\theta} F_{(x)} \sin \varphi] \quad (42)$$

and

$$\mathbf{E} = \mathbf{E}_{(z)} + \mathbf{E}_{(x)} = \eta_0 \mathbf{H} \times \hat{\mathbf{r}} \quad (43)$$

resulting in Poynting vector $\mathbf{E} \times \mathbf{H}^*$:

$$\mathbf{S} = \eta_0 \frac{k^2 \hat{\mathbf{r}}}{16\pi^2 r^2} (|F_{(z)} \sin \theta - F_{(x)} \cos \theta \cos \varphi|^2 + |F_{(x)} \sin \varphi|^2), \quad (44)$$

which results in

$$\mathbf{S} = \eta_0 \frac{(kd)^2 \hat{\mathbf{r}}}{16\pi^2 r^2} |I^+|^2, \quad (45)$$

So that the total radiated power for a forward wave is

$$P_{rad} = \int_0^{2\pi} \int_0^\pi \sin \theta d\theta d\varphi r^2 \hat{\mathbf{r}} \cdot \mathbf{S} = 30\Omega |I^+|^2 (kd)^2 \quad (46)$$

The generalization for a non matched line carrying a current given in Eq. (14) is done like in Section II-B, and the pointing vector for the general case is

$$\mathbf{S} = \eta_0 \frac{(kd)^2 \hat{\mathbf{r}}}{16\pi^2 r^2} (|I^+|^2 + |I^-|^2 + 2 \cos(2\varphi) \Re\{I^+ I^{-*}\}), \quad (47)$$

where \Re means the real part. Like for a finite TL, the interference between the waves does not contribute to the radiated power because $\int_0^{2\pi} d\varphi \cos(2\varphi) = 0$, so that the powers radiated by the separate waves add up to:

$$P_{rad} = 30\Omega (kd)^2 (|I^+|^2 + |I^-|^2) \quad (48)$$

In addition, the separate forward or backward waves have the same radiation, because setting $I^+ = 0$ recovers the result in Eq. (45) with $I^+ \rightarrow I^-$, or in other words a wave traveling *into* the termination or *out of it* radiates the same, according to the current intensity. This is significant for explaining how the radiation process from a finite TL evolves into two semi-infinite TLs for very long lines, as shown in Figure 9.

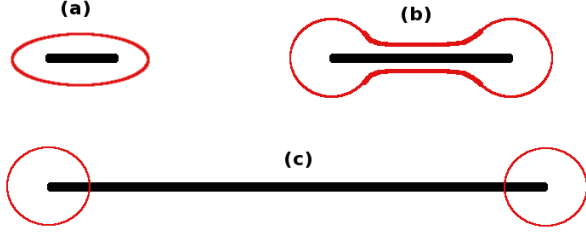


Fig. 9. Matched transmission lines carrying a forward wave. Panel (a) shows a short TL radiating the power $60\Omega(kd)^2|I^+|^2[1 - \text{sinc}(4kL)]$ according to Eq. (11). Panel (b) shows a TL longer than several wavelengths, for which $|\text{sinc}(4kL)| \ll 1$, which practically radiates $60\Omega(kd)^2|I^+|^2$, but still as a single radiating element. Panel (c) shows a TL longer than several thousands of wavelengths, for which the left termination is considered a semi-infinite TL from which the wave emerges and the right termination is considered a semi-infinite TL into which the wave enters, each semi-infinite TL radiates $30\Omega(kd)^2|I^+|^2$ according to Eq. (46).

V. RADIATION MODEL FOR TL

The radiation process can be incorporated in the RLGC model, by a series resistance per length unit R_{rad} . The radiation losses model is for a forward (or backward) wave, but given the interference between the waves does not contribute to the radiation, the model is accurate for any combination of waves. So let us consider a forward wave of current phasor I^+ .

As we saw in the previous section, the radiation can be attributed to the terminations of the TL, hence the radiation model must be symmetric around the middle of the line (at $z = 0$), specifically let us call the radiation resistance per length unit at the terminations $R_{\text{rad}}(\pm L)$. Hence $2|I^+|^2 R_{\text{rad}}(\pm L)dL$ is the *additional* radiated power if increasing the line length from $2L$ to $2(L + dL)$:

$$P_{\text{rad}} [2(L+dL) \text{ line}] - P_{\text{rad}} [2L \text{ line}] = 2|I^+|^2 R_{\text{rad}}(\pm L)dL \quad (49)$$

This implies the derivative of P_{rad} in Eq. (11) with respect to L , obtaining:

$$R_{\text{rad}}(\pm L) = 30\Omega(kd)^2 \frac{\text{sinc}(4kL) - \cos(4kL)}{L}, \quad (50)$$

Here we may replace L by any positive value of z along the TL. Given the model is symmetric around the middle of the line, it is convenient to define s the distance from the termination of the TL up to the *middle* of the transmission line (or to infinity for a semi-infinite TL). In terms of s

$$R_{\text{rad}}(s) = 30\Omega(kd)^2 \frac{\text{sinc}(4ks) - \cos(4ks)}{s} \quad (51)$$

The behavior of the normalized $R_{\text{rad}}(s)$ for a semi-infinite TL is shown in Figure 10. This model reproduces the correct radiation power, since

$$|I^+|^2 \int_0^\infty R_{\text{rad}}(s)ds = 30\Omega(kd)^2|I^+|^2 \quad (52)$$

Clearly, to describe the correct radiation losses, $R_{\text{rad}}(s)$ must also have negative values, due to the oscillatory behavior of the radiated power as function of the TL length. But this does not represent any problem, because the overall losses come out always positive.

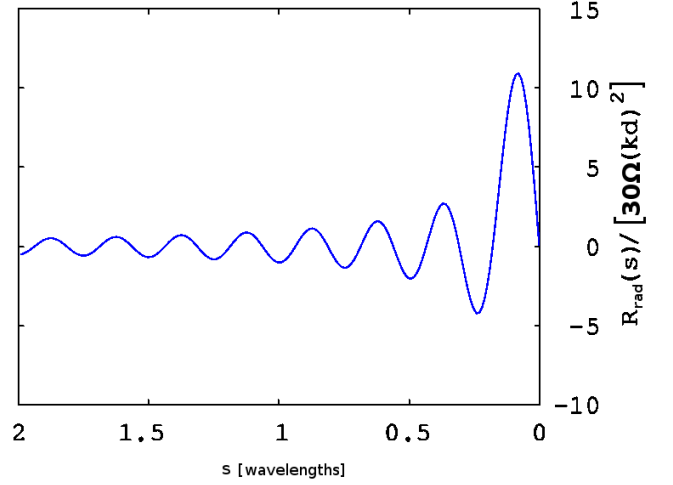


Fig. 10. Normalized value of the radiation resistance per length unit $R_{\text{rad}}(s)$ for a semi-infinite transmission line. The parameter s is the distance from the TL termination point, and is defined to infinity in this case. $R_{\text{rad}}(s)$ is linear with s for small s , while for big s it oscillates around 0 till it practically becomes 0 far from the termination of the TL.

For a finite TL, we set $R_{\text{rad}}(s)$ in Eq. (51) from each side up to the middle of the TL. Hence if the TL length is $2L$, $0 \leq s \leq L$ from each side, as shown in Figure 11 and the

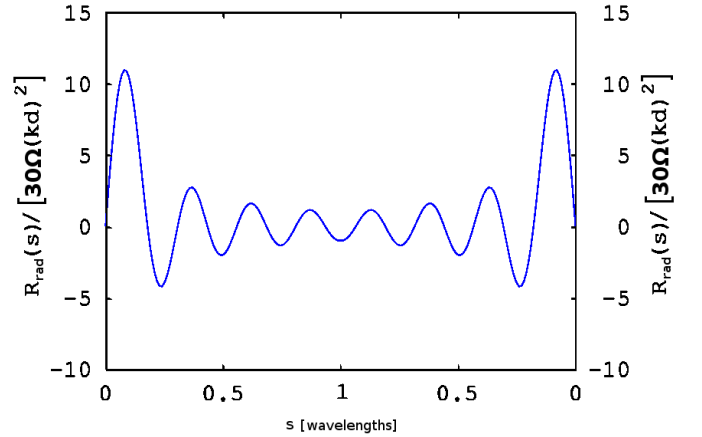


Fig. 11. Same as in Figure 10, only that for a finite TL of length $2L$, s measures the distance from each termination, up to the middle of the line, so that $0 \leq s \leq L$. In this example, L is one wavelength.

model describes correctly the radiation power since

$$|I^+|^2 \int_{-L}^L R_{\text{rad}}(s)ds = 2|I^+|^2 \int_0^L R_{\text{rad}}(s)ds = 60\Omega(kd)^2|I^+|^2[1 - \text{sinc}(4kL)] \quad (53)$$

Unlike in the case of ohmic or dielectric losses, for which the RLGC losses model is accurate only for a separate forward or backward wave, the radiation model is accurate for any combination of waves, because as we saw in the previous sections, the interference between the waves does not contribute to the radiation.

VI. CONCLUSIONS

We derived in this work a general radiation losses model for two conductors transmission lines (TL) in free space. The model defines the radiation resistance per length unit R_{rad} as function of the location on the TL, specifically as function of the distance to the nearest termination.

To attain this goal we derived in Section II a general expression for the power radiated by a finite TL, and validated our theoretical results in Section III with ANSYS HFSS commercial simulation results and by comparisons with other published works. We obtained an additional validation in Section IV where we derived a general expression for the power radiated by a semi-infinite TL, and we showed that a very long (finite) TL can be regarded as two semi-infinite TLs.

The analysis of an infinite and semi-infinite TL in Section IV shows that essentially the radiation from TL is a “termination effect” in the sense that the radiation originates at the termination, in analogy with OTR [14], [15], for which one defines a “formation length”, i.e. a region before the electron hits the discontinuity, in which the radiation formates. The analogue of this formation length in our case is the length for which $|\text{sinc}(4kL)| \ll 1$ in Eq. (11), where one reaches the asymptotic radiated power of two semi-infinite TLs. For example if one’s criterion is to reach the asymptotic value up to 1%, the corresponding distance to the termination is around 4 wavelengths, being the analogue of the formation length in OTR.

We remark that the radiated power increases in general with the increase in the TL length, but not monotonically, i.e. there are regions where it decreases, see Eq. (11) and Figures 4 and 7. This is due to the fact that the radiation is not a local process but rather a global process of constructive interference. For this reason, the radiation resistance per length unit R_{rad} is not always positive and that is the way to describe exactly the radiation effect. Certainly, the overall integral on the radiation resistance per length unit R_{rad} is always positive, the total radiated power being positive.

Extensions to this radiation model for TL in dielectric insulator and for multiconductor transmission lines (MTL) are in an advanced stage of study and will be published separately. The case of TL in dielectric insulator is solvable analytically, but much more involved than the free space case. The fact that the TL propagation wavenumber β is different from the free space wavenumber k by itself complicates the mathematics, but in addition it comes out that one needs to consider in this case also polarization currents (which have not been taken into account in [7]). We compared as well our analytic result (excluding polarization currents) for the case $\beta/k = 2$ with the dashed line in Figure 6 of Ref. [7] (called $K = 2$), and got a total overlap, which is encouraging.

APPENDIX A FAR VECTOR POTENTIAL OF SEPARATED TWO CONDUCTORS TRANSMISSION LINE IN TWIN LEAD REPRESENTATION

We show in this appendix that for the purpose of calculating the far fields from a two ideal conductor transmission line (TL)

in free space, having a well defined separation between the conductors, as shown in Figure 1, one can use an equivalent twin lead, provided the separation is much smaller than the wavelength.

For simplicity we use a forward wave (propagating like e^{-jkz}), but the same conclusion is valid for a combination of waves. In the far field the z directed magnetic potential vector A_z is expressed as

$$A_z = \mu_0 \int_{z_1}^{z_2} dz' \oint dc K_z(c) e^{-jkz'} G(R) \quad (\text{A.1})$$

where the dz' integral goes on the whole length of the TL,

$$G(s) = \frac{e^{-jks}}{4\pi s} \quad (\text{A.2})$$

is the 3D Green’s function, K_z is the surface current distribution as function of the contour parameter c (i.e. c_1 and c_2 , see Figure 1) which is known from electrostatic considerations, and R is the distance from the integration point on the contour of the conductors to the observer:

$$R = \sqrt{(x - x'(c))^2 + (y - y'(c))^2 + (z - z')^2}. \quad (\text{A.3})$$

Changing variable $z'' = z' - z$ in Eq. (A.1), one obtains

$$A_z = \mu_0 e^{-jkz} \int_{z_1-z}^{z_2-z} dz'' \oint dc K_z(c) e^{-jkz''} G(R), \quad (\text{A.4})$$

redefining $R = \sqrt{(x - x'(c))^2 + (y - y'(c))^2 + (z'')^2}$. For a far observer, at distance $\rho \equiv \sqrt{x^2 + y^2}$ from the TL, so that ρ is much bigger than the transverse dimensions of the TL one approximates R in cylindrical coordinates as

$$R \simeq r - \frac{\rho}{r} [x'(c) \cos \varphi + y'(c) \sin \varphi], \quad (\text{A.5})$$

where $r(z'') \equiv \sqrt{(z'')^2 + \rho^2}$. We keep for now everything in cylindrical coordinates, to be able to handle infinite or semi-infinite lines. Using this in Eq. (A.1), one obtains

$$A_z = \mu_0 e^{-jkz} \int_{z_1-z}^{z_2-z} dz'' \frac{e^{-jk[z'' + r(z'')]}{4\pi r(z'')}}{\oint dc K_z(c) e^{jk(\rho/r)[x'(c) \cos \varphi + y'(c) \sin \varphi]}. \quad (\text{A.6})$$

We consider the higher modes to be in deep cutoff, so that $kx'(c), ky'(c) \ll 1$, hence

$$A_z \approx \mu_0 e^{-jkz} \int_{z_1-z}^{z_2-z} dz'' \frac{e^{-jk[z'' + r(z'')]}{4\pi r(z'')}}{\oint dc K_z(c) \{1 + jk(\rho/r)[x'(c) \cos \varphi + y'(c) \sin \varphi]\}}. \quad (\text{A.7})$$

Separating the contour integral $\oint dc = \oint dc_1 + \oint dc_2$, where $c_{1,2}$ are the contours of the “upper” and “lower” conductors respectively (see Figure 1), and using

$$\oint dc_1 K_z(c_1) = - \oint dc_2 K_z(c_2) = I^+ \quad (\text{A.8})$$

so that the integral on each surface current distribution results in the total current, which we call I^+ , because it represents a forward wave. This current is equal, but with opposite signs on the conductors. We may define the 2D vector $\rho(c) \equiv$

$(x'(c), y'(c))$, from which one defines the vector distance between the center of the surface current distributions

$$\mathbf{d} \equiv \left[\oint dc_1 K_z(c_1) \rho(c_1) + \oint dc_2 K_z(c_2) \rho(c_2) \right] / I^+. \quad (\text{A.9})$$

From this point, the original cross section is relevant only for calculating the equivalent separation vector \mathbf{d} in the twin lead representation, and the remaining calculation bases solely on this *twin lead* representation. In appendix B we show examples for the calculation of the twin lead equivalent for given cross sections.

Using the twin lead representation, Eq. (A.7) may be rewritten

$$A_z = \mu_0 e^{-jkz} I^+ jk [d_x \cos \varphi + d_y \sin \varphi] \int_{z_1-z}^{z_2-z} dz'' \frac{e^{-jk[z''+r(z'')]}}{4\pi r(z'')} \frac{\rho}{r(z'')}, \quad (\text{A.10})$$

where d_x and the d_y are the x and y components of the vector \mathbf{d} . This represents a twin lead, as shown in Figure 2, and is actually a 2D dipole approximation of the TL. Without loss of generality, one redefines the x axis to be aligned with \mathbf{d} , so that $d_x = d$ and $d_y = 0$, obtaining

$$A_z = \mu_0 e^{-jkz} I^+ jkd \cos \varphi \int_{z_1-z}^{z_2-z} dz'' \frac{e^{-jk[z''+r(z'')]}}{4\pi r} \frac{\rho}{r(z'')}, \quad (\text{A.11})$$

which is equivalent of having a current $I^+ e^{-jkz}$ confined on the conductor at $x = d/2$ and the same current confined on the conductor $x = -d/2$ but defined in the opposite direction, representing a twin lead (see Figure 2). We are interested in radiation, so we require the observer to be many wavelengths far from the TL: $k\rho \gg 1$ and $kr \gg 1$, so that Eq. (A.11) may be further simplified to

$$A_z = -\frac{\mu_0 I^+ e^{-jkz} d \cos \varphi}{4\pi} \frac{\partial}{\partial \rho} \int_{z_1-z}^{z_2-z} dz'' \frac{e^{-jk[z''+r(z'')]}}{r(z'')}. \quad (\text{A.12})$$

The dz'' integral results in the exponential integral function Ei as follows

$$A_z = -\frac{\mu_0 I^+ e^{-jkz} d \cos \varphi}{4\pi} \frac{\partial}{\partial \rho} \text{Ei} \left(-jk \left[z'' + \sqrt{(z'')^2 + \rho^2} \right] \right) \Big|_{z_1-z}^{z_2-z}, \quad (\text{A.13})$$

where the Ei function satisfies $d\text{Ei}(s)/ds = e^s/s$.

The twin lead geometry also allows us to use simple models for the termination currents in the x direction (see Figure 2), defining the x component of the magnetic vector potential, calculated as:

$$A_{x,1,2} = \pm \mu_0 I^+ \int_{-d/2}^{d/2} dx' e^{-jkz_{1,2}} G(R_{1,2}) \quad (\text{A.14})$$

where the indices 1,2 denote the contributions from the termination currents at $z_{1,2}$, respectively, see (see Figure 2) and the distances $R_{1,2}$ of the far observer from the terminations may be expressed in spherical coordinates, as follows:

$$R_{1,2} \simeq r - z_{1,2} \cos \theta - x' \sin \theta \cos \varphi, \quad (\text{A.15})$$

The integral (A.14) is carried out for $kd \ll 1$, resulting in

$$A_{x,1,2} = \pm \mu_0 I^+ dG(r) e^{-jkz_{1,2}(1-\cos \theta)} \quad (\text{A.16})$$

APPENDIX B COMPUTATION OF RADIATION PARAMETERS

To calculate the power radiated from a TL, of any cross section, one needs the separation vector \mathbf{d} , defined in Figure 1, calculated from Eq. (A.9). If one needs the normalized radiation due to a forward wave, one also needs to know the characteristic impedance Z_0 . Those are obtained with the aid of the ANSYS 2D ‘‘Maxwell’’ simulation, from an electrostatic analysis. We ran the 2D ‘‘Maxwell’’ simulation on two cross sections shown in Figure B.1. It is to be mentioned that

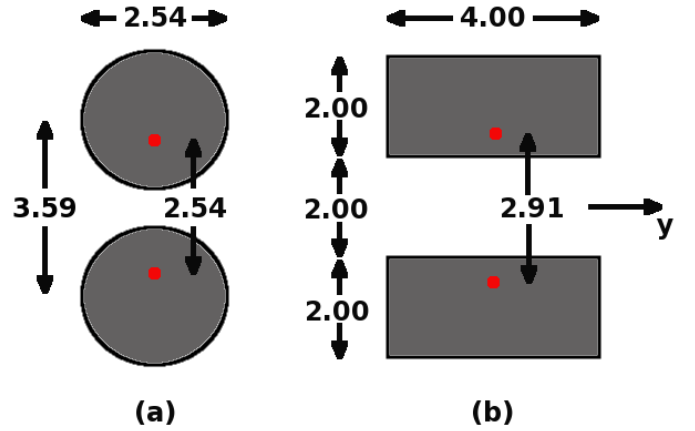


Fig. B.1. Panel (a) shows a cross section of circular shaped conductors and panel (b) shows a cross section of rectangular shaped conductors. The sizes are in units of cm. The y axis is horizontal, and the x axis for each cross section is the symmetry axis. The red points show the current images which define the twin lead representation, and are referred further on.

we know the analytic solution for the cross section in panel (a) from image theory [2], so that it can be used as a test for the quality of the numerical simulation. The magnitude of the electric fields measured for those cross sections is shown in Figure B.2. We remark that the surface currents,

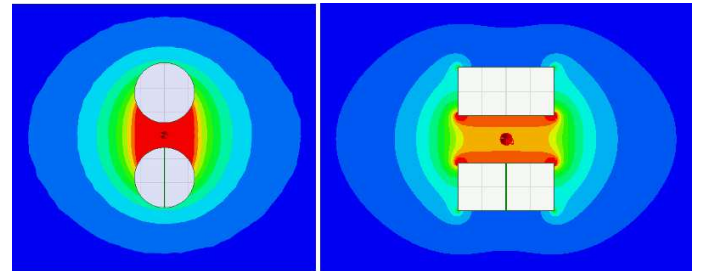


Fig. B.2. The magnitude of the electric field, the hottest color representing high field and coldest color low (close to 0) field, for the circular shaped conductors cross section in the left panel and for the rectangular shaped conductors in the right panel.

which are proportional to the (tangential) magnetic field on the conductors are also proportional to the (normal) electric field on the conductors. Given the surface currents $K_z(c_1) > 0$ and $K_z(c_2) < 0$ in Eq. (A.9), and using the field intensity which is positive, $E(c_1)$ is proportional to $K_z(c_1)$ and $E(c_2)$ is proportional to $-K_z(c_2)$, we may calculate the separation

vector \mathbf{d} , using Eqs. (A.8) and (A.9), after replacing $K_z(c_1)$ by $E(c_1)$ and $K_z(c_2)$ by $-E(c_2)$ as follows

$$\mathbf{d} = \frac{\oint dc_1 E(c_1) \boldsymbol{\rho}(c_1) - \oint dc_2 E(c_2) \boldsymbol{\rho}(c_2)}{\oint dc_1 E(c_1)}. \quad (\text{B.1})$$

For the cross sections in Figure B.1, the “positive” and “negative” conductors are symmetric, so that a given location vector $\boldsymbol{\rho}(c_2)$ on the negative conductor, is the minus of the corresponding location vector $\boldsymbol{\rho}(c_1)$ on the positive conductor, and by symmetry the magnitudes of the electric fields $E(c_1) = E(c_2)$, so that we may drop the second integral in the nominator of Eq. (B.1), and multiply the result by 2. Also by symmetry the y component of \mathbf{d} comes out 0, so that $d = |\mathbf{d}| = d_x$ represents the distance between the “image” currents in the twin lead model, and we obtained $d = 2.54$ cm for the circular cross section, and $d = 2.91$ cm for the rectangular cross section, as shown in Figure B.1.

We obtained from the 2D “Maxwell” simulation also the per length unit capacitances, which came out 31.5 pF/m and 33.51 pF/m for the circular and rectangular cross sections, respectively. The characteristic impedance Z_0 is calculated by $1/(Cc)$, where c is the velocity of light in vacuum and C is the per length unit capacitance, and come out 105.8Ω and 99.51Ω for the circular and rectangular cross sections, respectively.

The procedure described in this section can be done for any cross section, and it supplies all the values needed to calculate the normalized radiation in Eq. (13). Its accuracy can be found by comparing the values obtained for d and Z_0 for the circular cross section, with the theoretical values obtained from image theory and they fit with an inaccuracy of less than 0.5%.

REFERENCES

- [1] D. M. Pozar, *Microwave Engineering*, Wiley India Pvt., 2009
- [2] Orfanidis S.J., *Electromagnetic Waves and Antennas*, ISBN: 0130938556, (Rutgers University, 2002)
- [3] S. Ramo, J. R. Whinnery and T. Van Duzer, *Fields and Waves in Communication Electronics*, 3rd edition, Wiley 1994
- [4] E. C. Jordan and K. G. Balmain, *Electromagnetic Waves and Radiating Systems*, 2nd edition, Prentice Hall 1968
- [5] C. Manneback, *Radiation from Transmission Lines*, *Transactions of the American Institute of Electrical Engineers*, Vol. XLII, pp. 289-301, (1923) ; C. Manneback, *Radiation from Transmission Lines*, *Journal of the American Institute of Electrical Engineers*, 42(2), pp. 95-105, (1923)
- [6] G. Bingeman, *Transmission lines as antennas*, *RF Design* 2(1), pp. 74-82, (2001)
- [7] T. Nakamura, N. Takase and R. Sato, *Radiation Characteristics of a Transmission Line with a Side Plate*, *Electronics and Communications in Japan, Part I*, Vol. 89, No. 6, 2006
- [8] M. Bittera, V. Smiesko, K. Kovac, *Problem of Bundled Two-Wire Cable of Tested Equipment in Emission Measurement*, *Radioengineering*, 15(4), (December 2006)
- [9] R. Ianconescu and V. Vulfin, *TEM Transmission line radiation losses analysis*, *Proceedings of the 46th European Microwave Conference, EuMW 2016, London, October 3-7 (2016)*
- [10] R. Ianconescu and V. Vulfin, *Simulation and theory of TEM transmission lines radiation losses*, *ICSEE International Conference on the Science of Electrical Engineering*, Eilat, Israel, November 16-18 (2016)

- [11] A. Gover, R. Ianconescu, C. Emma, P. Musumeci and A. Friedman, *Conceptual Theory of Spontaneous and Taper-Enhanced Superradiance and Stimulated Superradiance*, *FEL 2015 Conference*, August 23-28, Daejeon, Korea, 2015
- [12] R. Ianconescu, E. Hemsing, A. Marinelli, A. Nause and A. Gover, *Sub-Radiance and Enhanced-Radiance of undulator radiation from a correlated electron beam*, *FEL 2015 Conference*, August 23-28, Daejeon, Korea, 2015
- [13] A. Gover, R. Ianconescu, A. Friedman, C. Emma and P. Musumeci, *Coherent emission from a bunched electron beam: superradiance and stimulated-superradiance in a uniform and tapered wiggler FEL*, *Nucl. Instr. Meth. Phys. Res. A*, <http://dx.doi.org/10.1016/j.nima.2016.12.038> (2016)
- [14] A. Nause, E. Dyunin, R. Ianconescu and A. Gover, *Exact Theory of Optical Transition Radiation in the Far and Near Zones*, *JOSA B*, 31(10), pp. 2438-2445, (2014).
- [15] V. L. Ginzburg, *Transition radiation and transition scattering*, *Physica Scripta Volume T*, 2:182, June 1982.
- [16] R. Ianconescu, *Radiation from charges in the continuum limit*, *AIP Advances*, 3 (6), (2013)
- [17] R. Ianconescu and L. P. Horwitz, *Energy mechanism of charges analyzed in real current environment*, *Foundations of Physics Letters*, Vol. 16, Number 3, pp. 225-244 (2003).
- [18] R. Ianconescu and L. P. Horwitz, *Self-Force of a Charge in a Real Current*, *Foundations of Physics Letters*, Vol. 15, Number 6, pp. 551-559 (December 2002).
- [19] R. Ianconescu and L.P. Horwitz, *Self-force of a classical charged particle*, *Physical Review A*, Vol. 45, Number 7, pp. 4346, (1992).
- [20] V. Vulfin and R. Ianconescu, *Transmission of the maximum number of signals through a Multi-Conductor transmission line without crosstalk or return loss: theory and simulation*, *IET MICROW ANTENNA P*, 9(13), pp. 1444-1452 (2015)
- [21] R. Ianconescu and V. Vulfin, *Simulation for a Crosstalk Avoiding Algorithm in Multi-Conductor Communication*, *2014 IEEE 28-th Convention of Electrical and Electronics Engineers in Israel, Eilat, December 3-5, (2014)*



Reuven Ianconescu graduated B.Sc (Summa cum laude) in 1987 and PhD in 1994, both in Electrical engineering at Tel Aviv university. He worked many years in R&D in the hi-tech industry, did a post-doc in the Weizmann Institute of Science, and is currently an academic staff member in Shenkar college of engineering and design. His research interests are: guided EM propagation, radiation and dynamics of charges and electrohydrodynamics.



Vladimir Vulfin has over 13 years of research experience in the areas of electromagnetic engineering. Since 2004 he worked in different companies as Electromagnetics Engineer. His job duties included design, simulations, implementations and measurements of antennas and microwave devices. Parallel to this, Vladimir was active as an external lecturer and instructor in different universities and colleges in Israel. He lead more than 100 degree final projects for students in Electrical Engineering Departments. Vladimir received the B.Sc and M.Sc. degrees in Electrical Engineering. Currently he is working towards his Ph.D degree at Ben Gurion University in the area of antennas and metamaterials.